PHYSICAL REVIEW A **88**, 041602(R) (2013)

Quantum systems of ultracold bosons with customized interparticle interactions

Alexej I. Streltsov

Theoretische Chemie, Physikalisch-Chemisches Institut, Universität Heidelberg, Im Neuenheimer Feld 229, D-69120 Heidelberg, Germany

(Received 25 April 2013; revised manuscript received 1 October 2013; published 21 October 2013)

Recent progress in cooling and trapping of polarized clouds of chromium ^{52}Cr, dysprosium ^{164}Dy, and erbium ^{168}Er opens a roadmap to quantum systems where the shapes of interparticle interactions can be customized. The main purpose of this work is to get deeper insight into the role the overall shape of the interparticle interaction plays in the context of trapped ultracold bosons. We show that strong interparticle repulsion inevitably leads to multihump fragmentation of the ground state. The fragmentation phenomenon is universal—it takes place in traps of different dimensionalities and topologies and for very broad classes of repulsive interparticle potentials. The physics behind this is identified and explained.

DOI: 10.1103/PhysRevA.88.041602 PACS number(s): 03.75.Hh, 05.30.Jp, 03.65.−w, 67.85.−d

Nowadays, dilute ultracold atomic and molecular clouds are considered as toolboxes to probe the static and dynamical properties of many-particle Hamiltonians [1–4]. Consequently, some phenomena which are very difficult or even impossible to study in their natural appearance and environment can be explicitly reconstructed and modeled in ultracold atomic systems. However, until recently, one substantial ingredient was missed—control over the overall shape of interparticle interactions.

Recent experiments with ultracold polarized clouds of chromium ^{52}Cr [5,6], dysprosium ^{164}Dy [7], and erbium ^{168}Er [8] have ultimately shown that the short-range interparticle interaction potential alone cannot describe the observed physics and it should be augmented by an additional long-range term which usually takes on the form of a dipole-dipole interaction [9,10]. Another venue to manipulate the effective interparticle interaction is to admix a small component of an excited Rydberg state to the ground state of ultracold atoms [11,12] via off-resonant optical coupling, thereby creating so-called "dressed" Rydberg systems. These steps towards the control and manipulation of the overall shape of the interparticle interaction open a roadmap to mimic or simulate static and dynamical phenomena and effects appearing in the context of other fields of physics where shapes of interparticle interactions play crucial roles, e.g., in nuclear physics.

The perspective of working with quantum systems where the interparticle interaction is customized encourages us to get deeper insight into the role it plays. The role of the sign is evident: If it is negative, the system is attractive, if it is positive, the system is repulsive, but what roles do its range and tails play? What physical phenomena or properties are they envisioned to impact? The main phenomenon predicted and intensively studied in the field of ultracold atoms is condensation, manifesting itself in a peaked density with a profile similar to the lowest-in-energy eigenstate of the confining potential. Condensation also means coherence between weakly interacting particles [1,2]. On the other hand, the existence of multihump features in the ground-state density might indicate possible (strong) correlations in the system which usually destroy condensation and break partially or completely the coherence between the particles.

The multihump structure of the ground-state density can be caused by applied external potential barriers. In a double well, for instance, a sufficiently high barrier can split the density into two well-separated subclouds. Such a system is then called twofold fragmented [13], implying that coherence between the subfragments is lost. If more barriers are available, as in optical lattices, the system can be multifold fragmented—in this respect, see the famous Mott-insulating phases [14]. Complimentary modulations of the density profiles and loss of interparticle coherence can be caused by a strong, repulsive interparticle interaction. In one-dimensional systems with contact interparticle interactions it originates from the well-known fermionization phenomenon [15,16] for interboson interactions of other shapes—to solidlike states [see, e.g., Coulomb bosons [17] and dipolar (screened Coulomb-like) bosons [18]]. In two dimensions strong repulsion is predicted to be responsible for so-called crystallization [9,10]—appearances of stable rims in the density profiles and/or its partial factorization into multihump structures (see, e.g., Refs. [19,20]). In [21], ground-state fragmentation of bosons with long-range interactions in a single trap has been shown to exist within a two-mode model.

The main goal of the present Rapid Communication is to investigate the microscopic details of how repulsive interparticle potentials create nontrivial features (humps) in the densities of ultracold systems confined in simple barrierless traps. We also want to understand which characteristic of a general interparticle interaction function favors these density modulations and, thereby, controls the accompanying developments of correlations and fragmentation.

Let us consider a generic many-body Hamiltonian of N identical bosons trapped in an external trap potential $V(\mathbf{r})$ and interacting via a general interparticle interaction potential: $\hat{H}(\mathbf{r}_1,\ldots,\mathbf{r}_N)=\sum_{j=1}^{N}[-\frac{1}{2}\nabla^2_{\mathbf{r}_j}+V(\mathbf{r}_j)]+\sum_{j<k}^{N}\lambda_0 W(\mathbf{r}_j-\mathbf{r}_k)$. Here λ_0 defines the strength of the interaction and $W(\mathbf{r}-\mathbf{r}')\equiv W(\mathbf{R})$ its shape. In this work, $\hbar=1, m=1$.

To start with, we consider several one-dimensional barrierless traps: a standard harmonic $V(x)=0.5x^2$, a nonharmonic $V(x)=0.5x^6$, and asymmetric linear $V(x)=\{-x: x<0; 3x/4: x\geqslant 0\}$. We examine the following interparticle interaction functions: exponential $\exp[-\frac{1}{2}(|x-x'|/D)^n]$, screened Coulomb $1/\sqrt{(|x-x'|/D)^{2n}+1}$, and sech-shaped $\mathrm{sech}[(|x-x'|/D)^n]$ of half-width D with $n=1$ and their *sharper* interactions analogous obtained with $n=2$. In the following we use the shorthand notations $\exp[-\mathbf{R}^n]$, $1/\mathbf{R}^n$, and $\mathrm{sech}[\mathbf{R}^n]$. To solve the respective many-boson Schrödinger equation numerically we use the recently developed

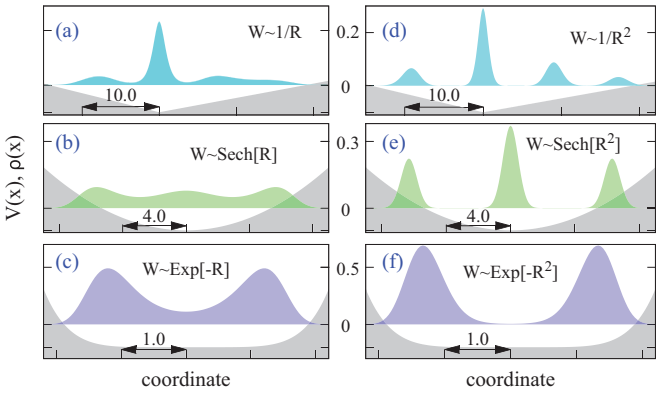

FIG. 1. (Color online) Diversity of fragmentation phenomena. Strong interparticle repulsion leads to the formation of multihump localized, fragmented structures irrespective of the shapes of the interparticle $W(\mathbf{R})$ and trapping $V(\mathbf{r})$ potentials used. Shown are the densities of one-dimensional systems made of $N = 108$ bosons and corresponding trapping potentials which are scaled and shifted for better presentation. Upper panels: Asymmetric linear trap and screened Coulomb interboson interactions of half-width $D = 5$ and strength $\lambda_0 = 0.3$ with $n = 1$ (a) and $n = 2$ (d). Middle panels: Harmonic trap and sech-shaped interactions with $D = 4$ and $\lambda_0 = 1.0$, $n = 1$ (b), $n = 2$ (e). Lower panels: Nonharmonic trap and exponential interparticle interactions with $D = 3$ and $\lambda_0 = 1.5, n = 1$ (c), $n = 2$ (f). Interparticle interaction potentials with *sharper* edges ($n = 2$) enhance fragmentation (see text for details). All quantities shown are dimensionless.

multiconfigurational time-dependent Hartree method for bosons (MCTDHB) [22,23]. This method is capable of providing numerically exact solutions [24].

The left panels of Fig. 1 plot the ground-state densities obtained at a full many-body level for one-dimensional systems with $1/\mathbf{R}$, sech[$\mathbf{R}$], and exp[$-\mathbf{R}$] interparticle interaction functions of different widths (ranges) confined in different traps. The main fascinating observation is that, irrespective of the shapes of the interparticle and trapping potentials used, a strong enough interparticle repulsion leads to the formation of multihump localized structures and, therefore, indicates possible correlations and fragmentation in the systems.

To shed more light on which characteristic parameters of the interparticle interaction function drive and control the number of humps, correlations and fragmentation, we have computed the ground-state properties of the same many-body systems as above, but with *sharper* interparticle interactions $1/\mathbf{R}^2$, sech[$\mathbf{R}^2$], and exp[$-\mathbf{R}^2$]. The results presented in the right panels of Fig. 1 show that for sharper versions of the interparticle interactions the multihump structures are retained and become even more pronounced. The many-body analysis of these multihump solutions reveals that they are not condensed but multifold fragmented (see Ref. [25] for more details). In the asymmetric linear trap the four-hump density of $N = 108$ bosons depicted in Fig. 1(d) is formed by four contributing natural subfragments $\rho(x) = \sum_{i=1}^{4} n_i |\phi_i^{\mathrm{NO}}(x)|^2$. The first fragment with $n_1 = 52$ bosons is localized at the trap minimum and forms the most intense hump. The leftmost hump is formed by $n_3 = 20$ bosons residing in a well-localized third natural orbital. Two other humps at the right are formed by $n_2 \approx 27.6$ and $n_4 \approx 8.4$ bosons residing in the second and fourth natural orbitals, which are slightly delocalized. In the harmonic trap and sech-shaped interaction [see Fig. 1(e)], the three symmetric fragments carry 30, 48, and 30 bosons, respectively. In the nonharmonic trap a Gaussian interaction results in a twofold fragmented ground state with 97.2 and 10.8 bosons per fragment [see Fig. 1(f)]. Here it is worthwhile to stress that for weak repulsions the regime of normal condensation is, of course, recovered irrespective of the particular form of interaction. Indeed, the ground-state density of the system depicted in Fig. 1(d) with a very weak repulsion $\lambda_0 = 0.01$ has one hump and is fully condensed, $n_1 \approx 100\%$ (see Ref. [25] for more details).

The above observed diversity of the fragmentation is caused by the interplay between the interparticle and trapping potentials. To distinguish and isolate effects originating from the range or width of the interparticle interaction, the particular shape of its tails, and the strength of the interparticle repulsion, let us consider a box-shaped trap and interparticle interaction potential of a rectangular shape, $W(x - x') = \{1 : |x - x'| \leqslant D; 0 : \text{otherwise}\}$. In this system an increase in the strength of the interparticle repulsion does not change either the effective length of the trap or the range of the interparticle interaction potential.

The left panels of Fig. 2 show how the ground-state densities of the system made of $N = 108$ bosons with a rectangular interparticle interaction of half-width $D = 3$, trapped in a box-shaped trap of length $L = 4$, respond when the repulsion strength is increased, $\lambda_0 = 0, 0.3, 1.0$. We see that in the noninteracting case the density is broad and has a maximum at the trap center. The strong interparticle repulsion, in contrast, leads to localization of the density at the edges of the box. Basic "electrostatic" arguments can explain this behavior. For strong

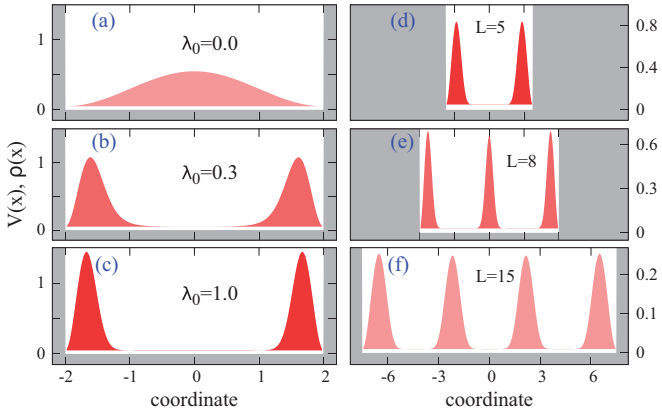

FIG. 2. (Color online) Physics of fragmentation in bosonic systems confined in box-shaped traps of length L and interacting via an interparticle interaction potential of rectangular shape with half-width $D = 3$. The left panels show that for strong repulsion $\lambda_0 = 0.3, 1.0$ [(b), (c)] it costs energy to keep $N = 108$ bosons in the middle of the trap ($L = 4$), and to minimize the energy the system fragments into two well-separated subclouds. The density of the noninteracting system is shown in (a). The right panels show how to control the fragmentation in strongly repulsive systems ($\lambda_0 = 1.0$) by varying the length L of the box. For $L = 8$ the ground state is threefold fragmented (e) and for $L = 15$ it is fourfold fragmented (f). Shown are the one-particle densities and trap potentials. All quantities shown are dimensionless.

repulsion it costs energy to keep the bosons in the middle of the trap, so they repel and push each other away—the cloud starts to form a minimum in the center of the trap. If we increase the repulsion further, the total energy is increased, but the system cannot expand farther apart due to the box-shaped topology of the trap. To minimize the energy the density is split into two well-separated fragments.

The right panels of Fig. 2 present a complimentary study where we keep the interparticle interaction $\lambda_0 = 1.0$, $D = 3$ fixed and increase the box size $L = 5,8,15$ providing, thereby, more room for the bosons. We see that starting from some critical length of the trap (box size), to minimize the repulsion, the system of $N = 108$ bosons is split into three subclouds with 36 bosons per fragment. To split the system into four fragments with 27 bosons per subcloud one has to increase the trap's length farther on. So, for strong enough interparticle repulsions, ground-state fragmentation is an inevitable property of trapped bosonic systems. The interplay between the width of the finite-range part of the interparticle interaction function and the length of the trap defines the particular fragmentation scenario.

To get deeper insight into the physics behind the fragmentation discovered above at a full many-body level, let us now rely on an idealized picture of a twofold fragmented state. The total density of such a state is formed by a sum of two isolated and independent subclouds (fragments). Its many-body wave function is then a Fock state $|n_1,n_2\rangle$ represented by a single symmetrized permanent $\Psi(\mathbf{r}_1,\ldots,\mathbf{r}_N) = \hat{\mathcal{S}}\phi_L(\mathbf{r}_1)\cdots\phi_L(\mathbf{r}_{n_L})\phi_R(\mathbf{r}_{n_L+1})\cdots\phi_R(\mathbf{r}_{n_L+n_R})$, with n_L bosons residing in the left ϕ_L and n_R in the right ϕ_R fragment, respectively. The optimal shapes of the fragments are determined self-consistently by solving the multiorbital best mean-field (BMF) equations [26,27] which we can be rewritten [25] as

$$\left[\hat{h} + \lambda_0(n_L - 1)V^{\rm eff}_{\phi_L}(\mathbf{r}) + \lambda_0 n_R V^{\rm eff}_{\phi_R}(\mathbf{r})\right]\phi_L = \mu_{11}\phi_L + \mu_{12}\phi_R,$$
$$\left[\hat{h} + \lambda_0(n_R - 1)V^{\rm eff}_{\phi_R}(\mathbf{r}) + \lambda_0 n_L V^{\rm eff}_{\phi_L}(\mathbf{r})\right]\phi_R = \mu_{21}\phi_L + \mu_{22}\phi_R.$$

Here $\hat{h} = -\frac{1}{2}\nabla^2_{\mathbf{r}} + V(\mathbf{r})$ is a single-particle Hamiltonian. The $V^{\rm eff}_{\phi_i}(\mathbf{r}) = \int |\phi_i(\mathbf{r}')|^2 W(\mathbf{r}-\mathbf{r}')d\mathbf{r}'$ terms play the roles of effective *self-consistent* potentials—their profiles depend on a given shape of interparticle function $W(\mathbf{r}-\mathbf{r}')$ and on the left and right densities $|\phi_i(\mathbf{r}')|^2$, $i = L,R$ of the involved subclouds. A negligible overlap between the well-isolated left and right fragments allows one to neglect the other integrals appearing in the original BMF equations.

The upper panel of Fig. 3 exemplifies schematically how the effective barrier $V^{\rm eff}_f = \int |f(x')|^2 W(x-x')dx'$ is produced by a rectangular interparticle interaction potential $W(x-x')$ of range D acting on a Gaussian-shaped cloud $f(x)$ of half-width a. This effective barrier depicted by a solid line with circles is centered at the cloud origin. The profile of this barrier is flat over the extent of the cloud $f(x)$ and drops as an **erf** function at the $\pm D$ edges.

Two other panels of Fig. 3 show how a rectangular interparticle interaction of half-width D induces the effective potentials in the above studied one-dimensional bosonic system trapped in a box-shaped trap. The lower panel of Fig. 3 depicts by a solid line with circles the interaction-induced effective potential $V^{\rm eff}_{\phi_L}(x) = \int |\phi_L(x')|^2 W(x-x')dx'$. It is constant over the extent of the $\phi_L(x)$ fragment and, therefore,

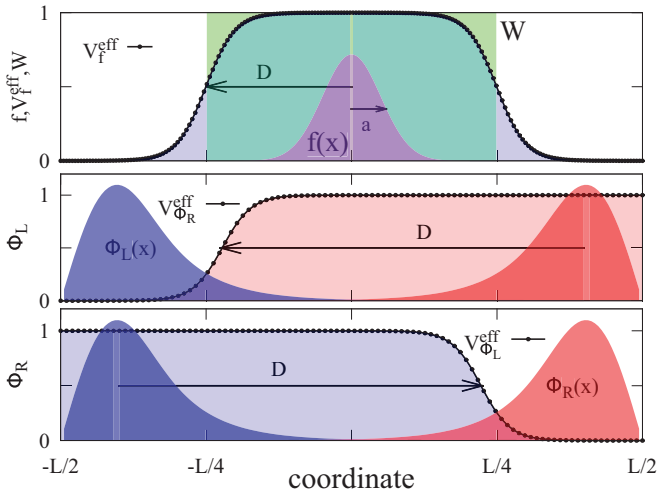

FIG. 3. (Color online) Explanation on how finite-range interparticle interaction potentials induce effective barriers and confine fragmented states. The upper panel plots by a solid line with circles an effective barrier $V^{\rm eff}_f(x) = \int |f(x')|^2 W(x-x')dx'$ produced by a rectangular interparticle interaction potential $W(x-x')$ of half-width D acting on a Gaussian-shaped function $f(x)$ of half-width a. Lower panel: The solid line with circles depicts an effective barrier $V^{\rm eff}_{\phi_L}(x) = \int |\phi_L(x')|^2 W(x-x')dx'$ produced by the action of a rectangular interparticle potential on the subcloud ϕ_L. The superposition of this interaction-induced effective barrier and the external trap (here it is a square box of length L) results in a well where the ϕ_R subcloud is confined. Middle panel: The action of the same finite-range $W(x-x')$ on ϕ_R produces an effective well capable of confining the left subcloud ϕ_L. The induced potential $V^{\rm eff}_{\phi_R}(x)$ is plotted by a solid line with circles. All quantities shown are dimensionless.

in the above BMF equations it just energetically shifts the left-localized subcloud upwards without changing its shape: $V^{\rm eff}_{\phi_L}(x)\phi_L(x) \approx \int |\phi_L(x')|^2 dx' \phi_L(x) = \phi_L(x)$. The action of $V^{\rm eff}_{\phi_L}(x)$ on the right fragment $\phi_R(x)$, in contrast, is dramatic—it induces the effective barrier. A superposition of this effective barrier and the external trap (box) is capable of confining the right subcloud $\phi_R(x)$. Similarly, the action of $W(x-x')$ on the right subcloud creates an effective barrier $V^{\rm eff}_{\phi_R}(x)$ confining the left fragment (see the middle panel of Fig. 3).

Here we have arrived at a microscopic, self-consistent picture of *self-induced* fragmentation which requires, as a prerequisite, localized subclouds, finite-range interparticle repulsion, and a trap of a finite length. The action of a finite-range repulsive interparticle potential on a cloud produces an effective barrier. The profile of this barrier depends on the density of the cloud, the number of the particles in it, and on the shape of $W(\mathbf{r}-\mathbf{r}')$. When several localized clouds or fragments are present, each of them creates its own effective potential that is seen by the other subclouds as an effective barrier. The superposition of these self-induced barriers and external trap results in a multiwell potential confining the fragmented system as a whole object.

The multihump structure of the density is driven by the fragmentation phenomenon, which has been observed experimentally [28,29] and is well understood theoretically [13,30–32]. From this perspective, variations of the shapes of $W(\mathbf{r}-\mathbf{r}')$ can modify the induced effective potentials and, thereby, the

fragmentation in the following manner: (a) By decreasing the range of the interparticle repulsion we increase the overlap between the fragments which reduces the fragmentation and leads to the development of coherence between them [33]; (b) by increasing the strength of the interparticle repulsion and keeping its range fixed we increase the heights of the induced barriers which isolate the fragments and enhance fragmentation; and (c) by flattening the tails of the interparticle interaction function one stimulates the overlap between the subclouds which melts the humps and blurs the fragmentation. A comparison of the left and right panels of Fig. 1 confirms this analysis.

A simple geometrical relation between the effective length of the trap L and range D of the finite-range part of the interparticle interaction function defines the number M of available humps (fragments). For $L < D$ we have a system of noninteracting particles because, irrespective of the shape and size of the trapped cloud, the created effective barrier is geometrically broader than the trap (box) itself. When $L > D$ there is enough room for two fragments to be trapped by the self-induced effective barriers; to accommodate M fragments the length of the trap should be $L > (M-1)D$ (see, e.g., Fig. 2).

The obtained geometrical picture of localized fragments and self-induced effective potentials is universal and can be applied to systems of bosons, fermions, and distinguishable particles also at higher dimensions. In the left and right panels of Fig. 4 we plot illustrative numerical examples of almost ideal self-induced twofold fragmented ground states of bosonic systems with $N = 100$ particles interacting via sharp repulsive sech-shaped interparticle potentials and confined in slightly elongated two- and three-dimensional harmonic traps.

Summarizing, we predict that the density of trapped repulsive ultracold bosons inevitably fragments into multihump structures to minimize strong interparticle repulsion. The physics behind this is an interplay between classical "electrostatic" repulsion which pushes the bosons from the trap center towards its edges, thereby provoking the formation of multihump structures in the density, and quantum mechanics which governs the loss of interhump coherence, i.e., fragmentation.

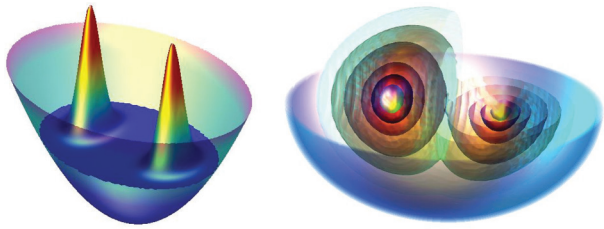

FIG. 4. (Color online) Universality of self-induced fragmentation mediated by finite-range interparticle interaction potentials. Left: Twofold fragmented ground state in a harmonic two-dimensional (2D) trap slightly elongated in one direction. Right: Twofold fragmented ground state in a slightly elongated three-dimensional (3D) harmonic trap. To visualize the 3D functions we plot several isosurfaces of the density and an equipotential cut of the trap. All quantities shown are dimensionless.

Finally, for experimental verification of the predicted phenomena with ultracold systems, one needs that (i) the range of interparticle interaction should be comparable with the length of trapping potentials and (ii) the repulsive interaction should be strong enough. Both these requirements are already reachable [25] within presently available technologies in dipolar ultracold atomic Bose-Einstein condensates trapped in tight optical traps [34,35] and in trapped ultracold systems of "dressed" Rydberg atoms [36,37].

I am grateful to Oksana I. Streltsova for 2D and 3D MCTDHB simulations, and to Ofir E. Alon, Lorenz S. Cederbaum, Luis Santos, and Michael Fleischhauer for fruitful discussions. Computation time on the bwGRiD and K100 clusters and financial support within the framework of the "Enable fund" of the excellence initiative at Heidelberg university are greatly acknowledged.

[1] F. Dalfovo, S. Giorgini, L. P. Pitaevskii, and S. Stringari, Rev. Mod. Phys. **71**, 463 (1999).
[2] A. J. Leggett, Rev. Mod. Phys. **73**, 307 (2001).
[3] T. Köhler, K. Góral, and P. S. Julienne, Rev. Mod. Phys. **78**, 1311 (2006).
[4] V. I. Yukalov, Phys. Part. Nucl. **42**, 460 (2011).
[5] A. Griesmaier, J. Werner, S. Hensler, J. Stuhler, and T. Pfau, Phys. Rev. Lett. **94**, 160401 (2005).
[6] J. Stuhler, A. Griesmaier, T. Koch, M. Fattori, T. Pfau, S. Giovanazzi, P. Pedri, and L. Santos, Phys. Rev. Lett. **95**, 150406 (2005).
[7] M. Lu, N. Q. Burdick, S. H. Youn, and B. L. Lev, Phys. Rev. Lett. **107**, 190401 (2011).
[8] K. Aikawa, A. Frisch, M. Mark, S. Baier, A. Rietzler, R. Grimm, and F. Ferlaino, Phys. Rev. Lett. **108**, 210401 (2012).
[9] M. A. Baranov, Phys. Rep. **464**, 71 (2008).
[10] T. Lahaye, C. Menotti, L. Santos, M. Lewenstein, and T. Pfau, Rep. Prog. Phys. **72**, 126401 (2009).
[11] J. E. Johnson and S. L. Rolston, Phys. Rev. A **82**, 033412 (2010).
[12] N. Henkel, R. Nath, and T. Pohl, Phys. Rev. Lett. **104**, 195302 (2010).
[13] P. Nozières and D. Saint James, J. Phys. France **43**, 1133 (1982).
[14] M. Greiner, O. Mandel, T. Esslinger, Th. W. Hänsch, and I. Bloch, Nature (London) **415**, 39 (2002).
[15] M. Girardeau, J. Math. Phys. **1**, 516 (1960).
[16] T. Kinoshita, T. Wenger, and D. S. Weiss, Phys. Rev. Lett. **95**, 190406 (2005).
[17] G. E. Astrakharchik and M. D. Girardeau, Phys. Rev. B **83**, 153303 (2011).
[18] F. Deuretzbacher, J. C. Cremon, and S. M. Reimann, Phys. Rev. A **81**, 063616 (2010).
[19] Yu. E. Lozovik, S. Yu. Volkov, and M. Willander, JETP Lett. **79**, 473 (2004).
[20] H. P. Büchler, E. Demler, M. Lukin, A. Micheli, N. Prokof'ev, G. Pupillo, and P. Zoller, Phys. Rev. Lett. **98**, 060404 (2007).
[21] Ph. Bader and U. R. Fischer, Phys. Rev. Lett. **103**, 060402 (2009).

[22] A. I. Streltsov, O. E. Alon, and L. S. Cederbaum, Phys. Rev. Lett. **99**, 030402 (2007).

[23] O. E. Alon, A. I. Streltsov, and L. S. Cederbaum, Phys. Rev. A **77**, 033613 (2008).

[24] A. U. J. Lode, K. Sakmann, O. E. Alon, L. S. Cederbaum, and A. I. Streltsov, Phys. Rev. A **86**, 063606 (2012).

[25] A. I. Streltsov, arXiv:1307.5187.

[26] L. S. Cederbaum and A. I. Streltsov, Phys. Lett. A **318**, 564 (2003).

[27] O. E. Alon, A. I. Streltsov, and L. S. Cederbaum, Phys. Lett. A **347**, 88 (2005).

[28] C. Orzel, A. K. Tuchman, M. L. Fenselau, M. Yasuda, and M. A. Kasevich, Science **291**, 2386 (2001).

[29] S. Hofferberth, I. Lesanovsky, B. Fischer, J. Verdu, and J. Schmiedmayer, Nat. Phys. **2**, 710 (2006).

[30] R. W. Spekkens and J. E. Sipe, Phys. Rev. A **59**, 3868 (1999).

[31] A. I. Streltsov, O. E. Alon, and L. S. Cederbaum, Phys. Rev. A **73**, 063626 (2006).

[32] E. J. Mueller, T.-L. Ho, M. Ueda, and G. Baym, Phys. Rev. A **74**, 033612 (2006).

[33] O. E. Alon, A. I. Streltsov, and L. S. Cederbaum, Phys. Lett. A **373**, 301 (2009).

[34] B. Pasquiou, G. Bismut, Q. Beaufils, A. Crubellier, E. Maréchal, P. Pedri, L. Vernac, O. Gorceix, and B. Laburthe-Tolra, Phys. Rev. A **81**, 042716 (2010).

[35] The ranges l_{dd} of the pure magnetic dipole-dipole interactions for ^{52}Cr, ^{164}Dy, and ^{168}Er atoms with magnetic moments of 6 μ_B, 10 μ_B, and 7 μ_B, respectively, are $l_{dd}^{\mathrm{Cr}} \sim 0.0024$ μm, $l_{dd}^{\mathrm{Dy}} \sim 0.0211$ μm, and $l_{dd}^{\mathrm{Er}} \sim 0.0106$ μm. These numbers can become comparable with the length l_{ω_L} of confinement potentials in lattice-induced traps. For an experimentally reachable [34] 130 kHz trap one gets $l_{\omega_L} \sim 16 l_{dd}^{\mathrm{Cr}}$, $l_{\omega_L} \sim 1.03 l_{dd}^{\mathrm{Dy}}$, and $l_{\omega_L} \sim 2.77 l_{dd}^{\mathrm{Er}}$. In this trap the strengths of the respective interactions are $\lambda_0 \sim 0.062$ for Cr, $\lambda_0 \sim 0.967$ for Dy, and $\lambda_0 \sim 0.491$ for Er, i.e., of the same order as used to get the multifold fragmented states depicted in Fig. 1.

[36] M. Viteau, M. G. Bason, J. Radogostowicz, N. Malossi, D. Ciampini, O. Morsch, and E. Arimondo, Phys. Rev. Lett. **107**, 060402 (2011).

[37] The range of the interaction between two "dressed" Rydberg atoms is controlled [11,12] by the so-called blockade radius R_c, which, as it was reported in a recent Rb experiment [36], can be 5–15 μm, whereas the length of the 100 Hz trap used in the transverse direction of the same experiment was 1–2 μm. The ratio between these numbers $l_{\omega_\perp} \sim 0.1 R_c^{\mathrm{Rb}}$ implies that, formally, the lengths and ranges needed to observe the predicted multihump multifold fragmented states are already reachable with ultracold "dressed" Rydberg atoms. The strength of this interaction can also be tuned in a quite broad range (see Refs. [11,12]).